Monthly Notices
of the
ROYAL ASTRONOMICAL SOCIETY

MNRAS **498,** 1023–1033 (2020)
Advance Access publication 2020 August 14

doi:10.1093/mnras/staa2435

Probing the atmosphere of HD189733b with the Na I and K I lines

E. Keles,[1]★ D. Kitzmann,[2] M. Mallonn,[1] X. Alexoudi,[1] L. Fossati,[3] L. Pino,[4,5] J. V. Seidel,[6] T. A. Carroll,[1] M. Steffen,[1] I. Ilyin,[1] K. Poppenhäger,[1] K. G. Strassmeier,[1] C. von Essen,[7] V. Nascimbeni[8,9] and J. D. Turner[10,11]

[1]*Leibniz-Institut für Astrophysik Potsdam (AIP), An der Sternwarte 16, D-14482 Potsdam, Germany*
[2]*University of Bern, Center for Space and Habitability, Gesellschaftsstrasse 6, CH-3012, Bern, Switzerland*
[3]*Space Research Institute, Austrian Academy of Sciences, Schmiedlstr. 6, A-8042 Graz, Austria*
[4]*Anton Pannekoek Institute for Astronomy, University of Amsterdam, Science Park 904, NL-1098 XH Amsterdam, The Netherlands*
[5]*INAF, Osservatorio Astrofisico di Arcetri, Largo Enrico Fermi 5, I-50125 Firenze, Italy*
[6]*Observatoire de l'Université de Genève, 51 chemin des Maillettes, CH-1290 Versoix, Switzerland*
[7]*Stellar Astrophysics Centre, Department of Physics and Astronomy, Aarhus University, Ny Munkegade 120, DK-8000 Aarhus C, Denmark*
[8]*Istituto Nazionale di Astrofisica, Osservatorio Astronomico di Padova, I-35122 Padova, Italy*
[9]*Dipartimento di Fisica e Astronomia, Universta di Padova, Vicolo dell Osservatorio 3, I-35122 Padova*
[10]*Cornell University, Ithaca, NY 14850, USA*
[11]*University of Virginia, Charlottesville, VA 22904, USA*

Accepted 2020 August 5. Received 2020 July 30; in original form 2020 May 22

ABSTRACT

High spectral resolution transmission spectroscopy is a powerful tool to characterize exoplanet atmospheres. Especially for hot Jupiters, this technique is highly relevant, due to their high-altitude absorption, e.g. from resonant sodium (Na I) and potassium (K I) lines. We resolve the atmospheric K I absorption on HD189733b with the aim to compare the resolved K I line and previously obtained high-resolution Na I-D line observations with synthetic transmission spectra. The line profiles suggest atmospheric processes leading to a line broadening of the order of ∼10 km/s for the Na I-D lines and only a few km/s for the K I line. The investigation hints that either the atmosphere of HD189733b lacks a significant amount of K I or the alkali lines probe different atmospheric regions with different temperature, which could explain the differences we see in the resolved absorption lines.

Key words: planets and satellites: atmospheres – planets and satellites: composition – planets and satellites: gaseous planets .

1 INTRODUCTION

The characterization of exoplanets and especially their atmospheres increases our understanding of planetary formation and evolution. One possibility to characterize exoplanets is transmission spectroscopy, thus inferring the fingerprints of planetary atmospheres (Seager & Sasselov 2000), as a part of the starlight is absorbed or scattered by atmospheric constituents during transit.

Using high-resolution spectroscopy (Snellen et al. 2010; Cauley et al. 2019; Yan et al. 2019), one can reveal information about sharp line absorption at high altitudes. These absorptions are investigated usually using either the so-called 'excess absorption method', where the flux of the spectral range of interest is integrated within a bandwidth and divided by the flux within a reference band (Charbonneau et al. 2002) or the 'division method', where the observations during the transit are divided by the mean of the out-of-transit observations (Wyttenbach et al. 2015), showing the spectrally resolved planetary absorption. The information inferred from the spectral lines can be used to determine different properties from the probed atmospheric region, e.g. the temperature profile (Wyttenbach et al. 2015), number densities (Huang et al. 2017), escape (Fossati et al. 2018), aerosols (Pino et al. 2018a,b), or the pressure level (Gibson et al. 2020; Turner et al. 2020). Absorption lines of interest are the alkali lines Na I and the K I with their strong absorption cross-sections (Lavvas, Koskinen & Yelle 2014), where the exoplanet HD189733b is one of the first exoplanets where atmospheric Na absorption was found (Redfield et al. 2008).

The exoplanet HD189733b has an apparent radius of $1.151 \times R_{\rm Jup}$ and an orbital period of 2.21 d. It orbits an active K-dwarf star with an apparent magnitude of $V = 7.7$ mag and a radius of $0.752 \times R_{\rm Sun}$. The first Na I detection in the atmosphere of HD189733b was presented by Redfield et al. (2008) using the high-resolution spectrograph instrument attached to the 9.2-m Hobby-Eberly-Telescope. An Na I excess absorption of 0.0672 ± 0.0207 per cent was found, as well as a blueshift in the planetary absorption signal within the transmission spectrum. The authors speculated that this was caused by high-speed winds flowing from the hot dayside to the cooler nightside of HD189733b. This result was confirmed by Wyttenbach et al. (2015) and Casasayas-Barris et al. (2017) using the ESO 3.6-m telescope and the High-Accuracy Radial velocity Planet Searcher (HARPS) spectrograph as well as by Khalafinejad et al. (2017) using

★ E-mail: ekeles@aip.de

© 2020 The Author(s)
Published by Oxford University Press on behalf of the Royal Astronomical Society

Downloaded from https://academic.oup.com/mnras/article/498/1/1023/5892592 by Universiteit van Amsterdam user on 15 March 2022

the Ultraviolet and Visual Echelle Spectrograph (UVES) instrument attached to the Very Large Telescope (VLT). Several investigations attempted to detect K on HD189733b. For instance, Jensen et al. (2011) used the Hobby–Eberly telescope but without success. A tentative 2.5-σ detection of K I in the atmosphere of HD189733b is shown by Pont et al. (2013) where the Advanced Camera for Surveys instrument onboard of the *Hubble Space Telescope* (*HST*) was used for their observations. Recently, Keles et al. (2019) detected K I with an excess level of 0.184 ± 0.022 per cent on HD189733b using the Large Binocular Telescope (LBT) and the Potsdam Echelle Polarimetric and Spectroscopic Instrument (PEPSI).

A particular emphasis is given to wind properties within the atmosphere of HD189733b, which are investigated in different high-resolution transit observations, e.g. Louden & Wheatley (2015), Brogi et al. (2016), Salz et al. (2018), or Seidel et al. (2020). Winds on giant exoplanets can vary, e.g. being equatorial jets that originate from the lower parts of an atmosphere (around 1 bar) and stream into the direction of the planet's rotation, day- to nightside winds that arise at higher altitudes (around 1 mbar) or atmospheric superrotation (Brogi et al. 2016). These winds can vary from planet to planet, as different effects have an influence on their atmospheric properties, e.g. a planetary magnetic field or synchronization between the atmosphere and the planet interior (Brogi et al. 2016). In the case of day- to nightside winds, the line cores of resolved absorption lines show a blueshift as the wind pushes the atmosphere into the observer's line of sight during transit. In the other cases, the absorptions arising from different positions on the observable annulus are velocity shifted regarding the projected distance to the rotation axis (largest shift on the greatest projected distance and lowest at the region where the atmosphere becomes opaque). On the trailing and leading limbs, the shift is of opposite direction (Louden & Wheatley 2015). The resulting observed final absorption line is the sum of each of these intrinsic shifted absorptions, which results in a broadened and shallower absorption line compared to an absorption line from a stagnant atmosphere. The aforementioned studies show a tentative consensus for the existence of an eastward equatorial jet in the atmosphere of HD189733b, which is consistent with modelling approaches [see Showman et al. (2013) and the references therein].

In this work, we spectrally resolve the atmospheric K I line on HD189733b from the observation presented by Keles et al. (2019) and compare the line shape to the resolved Na I-D lines presented by Casasayas-Barris et al. (2017). The alkali atoms Na and K are known to have very similar condensation curves as well as similar ionization potentials (Lavvas et al. 2014), leading to very similar-shaped mixing ratio profiles (Lavvas & Koskinen 2017). As the observations suggest a strong broadening of the Na I-D lines, also recently shown by Seidel et al. (2020) and Gebek & Oza (2020), we investigate the line widths by comparing them to synthetic line profiles. We discuss the difference in the broadening of the alkali lines and their possible trigger, such as winds. The comparison between the alkali lines enables us to discuss either a scenario where the alkali lines probe the same atmospheric region, which would hint on a supersolar planetary Na/K- ratio or a scenario where both features trace significantly different atmospheric regions with different temperature.

This paper is structured as follows. Section 2 shows the observational data and Section 3 shows the models used. The methods and results are presented in Section 4, where we resolve the K I-absorption and compare both alkali lines with synthetic transmission spectra. In Section 5, we compare the alkali lines with each other and discuss the results. Section 6 presents the summary and conclusion.

2 OBSERVATIONAL DATA

2.1 The K I observation

A transit of HD189733b was observed at the LBT with PEPSI, which is a white–pupil fibre-fed spectrograph (Strassmeier et al. 2015; Strassmeier, Ilyin & Steffen 2018a; Strassmeier, Ilyin & Weber 2018b). The observation covered the wavelength range of 7340–9070 Å at a 4-pixel spectral resolution of 130 000. During the observation, 15 out-of-transit and nine in-transit spectra were observed at an exposure time of 10 min. The telluric and blaze correction, as well as the image-processing steps, is described in detail in Keles et al. (2019) (hereafter KEL19). The authors found a significant K I-excess absorption for bandwidths between 0.8 and 8.0 Å around the K I line at 7698.98 Å in their observation. We use the processed and telluric-corrected data set from KEL19 and spline them to the wavelength grid with a spacing of 0.01 Å to resolve the planetary K I line at 7698.98 Å. The second resonant K I line at 7664.92 Å is contaminated by strong telluric oxygen lines and is not investigated.

2.2 Na I detection by Casasayas-Barris et al. (2017)

Casasayas-Barris et al. (2017) (hereafter CSB17) presented three transit observations of HD189733b acquired with the HARPS instrument (Mayor et al. 2003) with a resolution of ∼11 5 000 on the ESO 3.6-m telescope (La Silla Observatory). They comprised 99 spectra (46 being in-transit and 53 being out-of-transit) at exposure times of 5 min and 10 min. The authors find a significant Na I absorption resolved around both Na I-D lines at 5889.906 Å and 5895.879 Å. Although the detection of the Na I-D lines using the same data set is made first by Wyttenbach et al. (2015), we will compare the resolved K I line profile with the findings by CSB17, as the authors considered the effect of centre-to-limb variation (CLV) (see e.g. Czesla et al. 2015; Yan et al. 2017) and the Rossiter–McLaughlin (RM) effect (McLaughlin 1924; Rossiter 1924) in their investigation. For this, we use the unbinned resolved Na I-D-line profiles from CSB17 presented in their fig. 7 (top panel).

3 MODELS

3.1 The residual RM feature

Due to the stellar rotation, the stellar lines become shifted in wavelength according to their position on the stellar surface, whereby the line shifts decrease towards the stellar centre. During the transit, in case of HD189733, the planetary body blocks blue-shifted light during the first part of the transit and red-shifted light during the second part of the transit and hence introduces a line deformation and shift to the observed mean stellar line. This effect introduces a residual feature after dividing the in-transit spectra by the master out-of-transit spectrum, which we denote here as the 'residual RM feature.'

The shape of the residual RM feature in the transmission spectra depends strongly on the line properties of the investigated stellar line, the star–planet geometrical properties, and the stellar properties, e.g. stellar rotation velocity and obliquity. This side effect introduced by the RM effect is addressed in different investigations in the literature, e.g. Louden & Wheatley (2015), Brogi et al. (2016), and Chen et al. (2020) and especially in the recent work by Casasayas-Barris et al. (2020), showing the non-detection of Na I in the atmosphere of HD209458b and the importance to consider the RM effect.

Downloaded from https://academic.oup.com/mnras/article/498/1/1023/5892592 by Universiteit van Amsterdam user on 15 March 2022

We model the residual RM effect using a grid model, where we map the stellar surface by a grid of 100 x 100 pixels containing limb angle-dependent fluxes, thus considering also the CLV effect (for further information on the stellar spectra, we refer to Section 3.3 in KEL19). To account for the stellar rotation, each spectrum is shifted according to the differential velocity on the stellar surface. During the transit, the planetary surface (mapped by 70 x 70 pixels) blocks different regions of the stellar surface, leading to the aforementioned effect.

3.2 The rotational broadening model

We model the rotational broadening of the synthetic transmission lines using a grid model, where we map the planetary surface by a grid of 100 × 100 pixels containing the synthetic lines. To account for the rotational broadening, each spectrum is shifted according to the differential velocity on the planetary surface. The planetary surface consists of the planetary body (at 1 × R_p) and the probed atmospheric ring, where the absorption lines originate. To compute the broadened absorption line profile, we sum over all pixels on the atmospheric ring. We define the border of the atmospheric ring at 1.285 × R_p for the Na I-D2-line absorption at 1.200 × R_p for the Na I-D1-line absorption and at 1.136 × R_p for the K I line absorption inferred according to the line contrasts of the non-broadened line profiles derived in this work (see Section 5). Note that these boundaries are first-order approximations. However, the choice of the boundary has a small effect on the outcome, as the line broadening is determined mainly by the rotational velocity.

We validated our model by comparing it to the [1] PyAstronomy tool *pyasl.fastRotBroad*, which introduces rotational broadening according to (Gray & Corbally 1994) (i.e. for a stellar surface). We introduced different broadening values to synthetic line profiles, which show no significant deviations from each other for both models.

3.3 The synthetic transmission spectra

We will compare the alkali lines with line profiles from synthetic transmission spectra. The theoretical transmission spectra are calculated for different atmospheric temperatures and volume mixing ratios. The temperature is varied between 2000 and 6000 K in steps of 200 K. The volume mixing ratio for potassium is varied in the range around $\sim 10^{-9}-10^{-5}$ and the sodium volume mixing ratio in the range of $\sim 10^{-7}-10^{-3}$ around the solar composition values, which are $\sim 10^{-6}$ for Na and $\sim 10^{-7}$ for K (Pino et al. 2018a). The atmosphere of HD189733b is well known for showing a scattering slope in the visible wavelength region that is far larger than predicted by molecular Rayleigh scattering alone (e.g. Pont et al. 2013). A well-accepted explanation for this effect is the occurrence of small aerosol particles in the upper atmosphere that contribute to the scattering optical depth in this wavelength range. We follow the work of Pino et al. (2018a) [see their equation (10)] and include this aerosol scattering via analytic approximations, which are based on the *HST* spectra of HD189733b. The transmission spectra are calculated with a reference pressure of 10 bars located at the measured white light radius of HD189733b. Further details on the computation is provided in Appendix A.

All synthetic spectra were calculated with a spacing of 0.01Å similar to the spacing of the observational data and convolved with the instrumental resolution using the PyAstronomy tool *PyAstronomy.pyasl.instrBroadGaussFast*. As the synthetic transmission spectra mirror the wavelength-dependent radius (R_p) of HD189733b, we convert them via $1-(R_p/R_*)^2$, equivalent to the observational line profiles and normalize them with a second-order polynomial fit to the continuum from 5000Å to 10000Å.

[1] https://github.com/sczesla/PyAstronomy

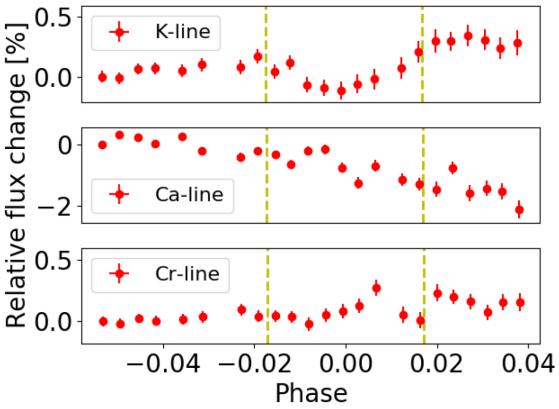

Figure 1. Excess absorption around a 0.5 Å bandwidth centred around the K I line at 7699 Å (first panel), the Ca II line at 8662 Å (second panel), and the control Cr I line at 7462 Å (third panel).

4 METHOD AND RESULTS

4.1 Re-investigating the K I absorption on HD189733b

We aim to spectrally resolve the planetary K I line and compare its line shape to the Na I-D lines presented in CSB17. Many processes can affect high-resolution transit spectra and need to be considered, e.g. telluric lines (see e.g. Allart et al. 2017), the CLV (see e.g. Czesla et al. 2015; Yan et al. 2017), the RM effect (see e.g. Cameron et al. 2010; Cegla et al. 2016; Dravins, Gustavsson & Ludwig 2018; Bourrier et al. 2018), or stellar activity (see e.g. Cauley et al. 2018), whereas the later is of main importance especially for this work and demonstrated in Fig. 1 (see below). To separate the planetary K I absorption from the stellar line profile, one needs to derive the transmission spectrum by dividing the in-transit spectra (the observations acquired during the transit) by a master out-of-transit spectrum (the mean spectrum of the observations acquired before and after the transit). We derive the master out-of-transit spectrum using 14 out-of-transit spectra, neglecting ingress and egress observations. The planetary motion introduces a Doppler shift to the wavelength position of the planetary absorption lines. Due to this, each transmission spectrum is shifted back to the planetary rest frame and the transmission spectra co-added, demonstrating the planetary absorption. The left-hand panel in Fig. 2 shows the transmission spectra subtracted by unity (orbital phase versus velocity shift). There is an emission-like feature increasing with planetary orbital phase, which is continuing also in the out-of-transit observations (visible beyond the green dashed lines that mark the first and fourth contacts). This is mentioned also by KEL19 and was related to stellar activity.

In order to investigate spurious stellar activity during the transit, Fig. 1 shows the excess absorption around the K I line at 7699 Å (top), the Ca II line at 8662 Å (second panel), and the control Cr I line at 7462 Å (third panel). The excess absorption derived here is the flux integrated around the line cores within a bandwidth of 0.5 Å and normalized using a linear fit to the out-of-transit values. To

Downloaded from https://academic.oup.com/mnras/article/498/1/1023/5892592 by Universiteit van Amsterdam user on 15 March 2022

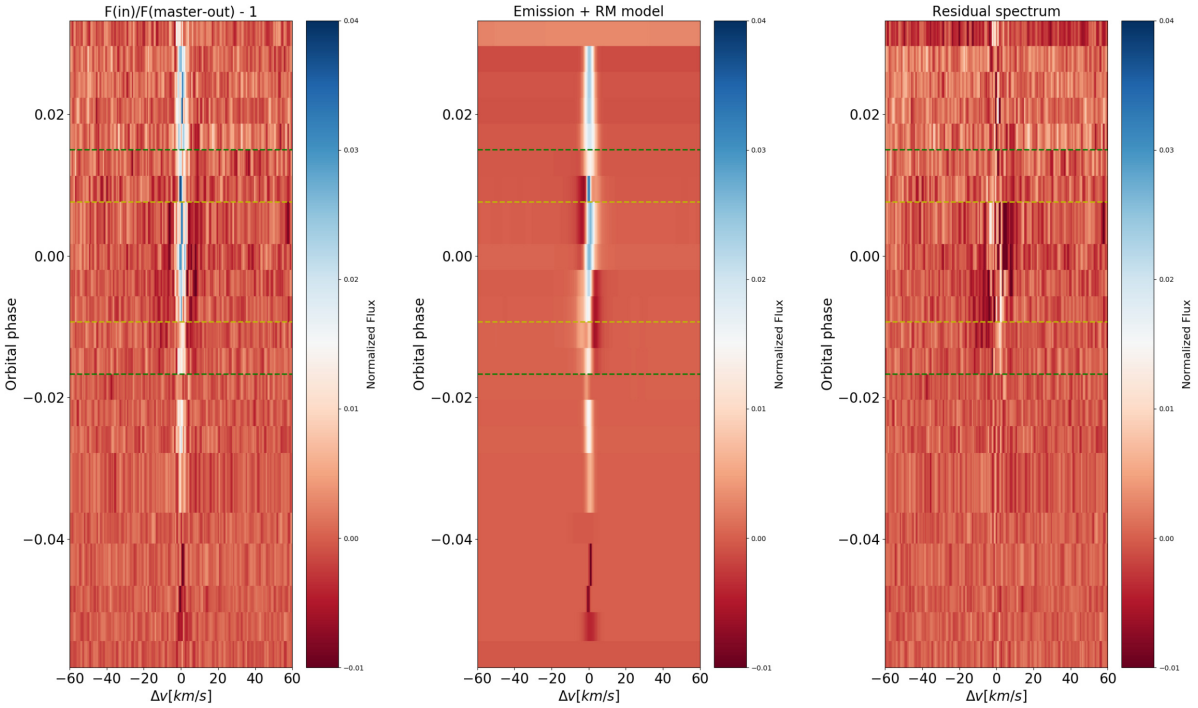

Figure 2. Transmission spectra around the K I line at 7698.98 Å (orbital phase versus velocity shift). Left-hand panel: The observations divided by the Master out spectrum and subtracted by unity (red). Middle panel: The residual RM model and the fit to the emission line induced by stellar activity. Right-hand panel: The residual spectrum (left-hand panel divided by the middle panel) showing the K I absorption (dark region). Green dashed lines mark the first and fourth contacts and the yellow lines the second and third contacts.

show the relative flux change, the values are divided again by the value of the first observation. As mentioned by KEL19, we see a slope in the top two excess curves, which can be well described by a linear fit. The Ca II-IR triplet lines are known to show variations due to stellar chromospheric activity. Klocová et al. (2017) investigated a flare during one transit of HD189733b determining a change in flux of the Ca II line at 8498 Å of around 2–3 per cent (see their fig. 6). Comparing this to Fig. 1, we see a decrease in flux of around 2 per cent in the Ca II line, showing a possible correlation with the activity. We show this correlation also for the weaker control Cr I line, which is less affected than the strong K I line.

To account for the emission feature and the residual RM feature (see Section 3.1) in the transmission spectra shown in the left-hand panel of Fig. 2, we fit the emission line with a Gaussian profile using the Pyastronomy tool *funcfit* and combine it with the residual RM feature model (middle panel in Fig. 2). Due to the low rotation velocity of 3.3 km/s of the host star HD189733, the residual RM feature does not move much and overlaps with the emission feature in the line core region. As the transit duration of around ∼109 min is quite short, there are only five transmission spectra available after neglecting the ingress and egress spectra, where the planetary absorption moves around ±8 km/s corresponding to ±0.21 Å.

The transmission spectra are subsequently corrected for the resulting model by division (right-hand panel in Fig. 2), showing the velocity-shifted planetary absorption at different orbital phases. To derive the final planetary transmission spectrum, we shift the in-transit transmission spectra corrected by the model to the planetary rest frame and co-add them. The final transmission spectrum is shown in Fig. 3. Applying a Gaussian fit (black solid line), we determine the full width at half-maximum (FWHM) = 0.24 ± 0.03 Å and the LC = 0.46 ± 0.04 per cent. The residual spectrum is shown with an offset (orange solid line), showing no correlated noise. We expect the line centre at 7698.965 Å (as we removed the systemic velocity of −2.277 km/s). The line centre is at 7698.966 ± 0.01 Å and shows no significant wavelength shift.

To verify our result, we calculate the K I excess absorption from the final transmission spectrum and compare it with the results of KEL19 for different integration bandwidths. For this, we integrate the final F_{in}/F_{out} spectrum around the line core and normalize it by the number of integrated points. The excess absorptions agree within their error bars up to 4.0-Å bandwidths and remain within three error bars for larger bandwidths. The deviations at larger bandwidths may arise due to the different techniques used to derive the excess absorption level (Casasayas-Barris et al. 2020).

4.2 Comparison of the synthetic and observational K I line profile

To investigate the K I line shape, we compare the resolved K I line with the line profiles from the synthetic transmission spectra. For this purpose, we calculate the reduced χ^2 value ±0.24 Å around the K I line core corresponding to ∼2× the FWHM (in total 48 spectrally resolved data points). Before the reduced χ^2-value calculation, we introduce rotational broadening to the synthetic line profiles according to Section 3.2 to account for line broadening. We increase this in steps of 0.1 km/s and calculate the reduced χ^2 value repeatedly until we reach a reduced χ^2 minimum between the observational and synthetic line profiles. We do this exercise for each synthetic temperature-abundance spectrum separately.

Here, we emphasize that high-resolution observations are insensitive to the atmospheric continuum and can measure only the contrast

Downloaded from https://academic.oup.com/mnras/article/498/1/1023/5892592 by Universiteit van Amsterdam user on 15 March 2022

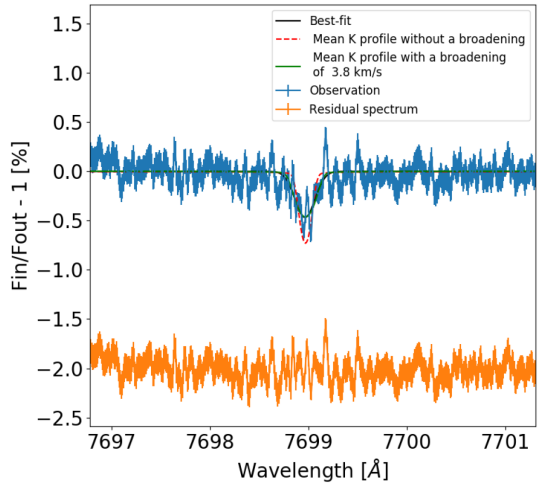

Figure 3. Transmission spectrum around the K I line at 7699 Å in (per cent) subtracted from unity. The black solid line shows the Gaussian fit. The dashed lines show the expected planetary absorption from the synthetic spectra without any broadening (red) and with the best-matching broadening solution of 3.8 km/s (green). The residual spectrum is shifted for clarity.

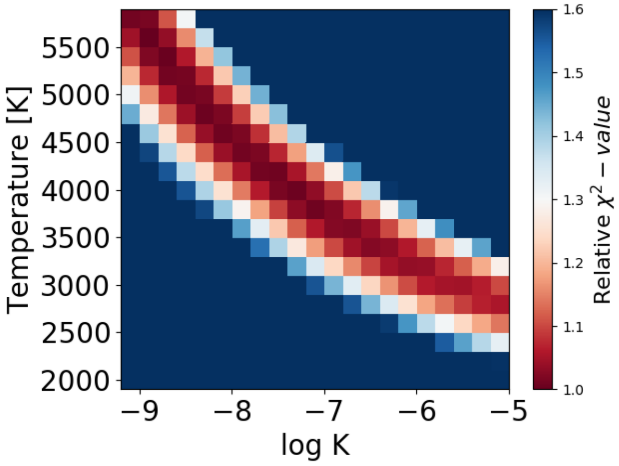

Figure 4. Shown is the abundance-temperature degeneracy for K I line. log K denotes the logarithmic volume mixing ratio of K. Reduced χ^2 values (colour marked) relative to the best value compare the observational K I line with various synthetic line profiles. Each pixel corresponds to one comparison.

of an absorbing feature, i.e. the difference between the line core and the continuum. This contrast does not change increasing (or decreasing) the abundance of a species, as the feature originates higher up (or lower down) in the atmosphere not changing its contrast (Pino et al. 2018a). In this work, the continuum (and thus the contrast) is set by the haze layer. Therefore, increasing the temperature or abundance shifts the absorption line higher up in the atmosphere, which arises more and more above the haze layer and mimics an increase in absorption for higher temperature and abundance.

The comparison map between the synthetic and observed K I line profile is shown in Fig. 4. Each pixel corresponds to one synthetic transmission spectrum and observation comparison. The colour bar shows the reduced χ^2 minimum value relative to the best value. The characteristic shape of the colour map highlights the degeneracy between the temperature and the K abundance. Increasing the temperature, the scale height increases as well and shifts the absorption to higher altitudes. Similarly, higher abundances lead to a stronger absorption signature above the haze layer, which reaches higher altitudes. Thus, an absorption feature induced by an increased temperature cannot be distinguished a priori by an absorption feature induced by higher abundance if the continuum is determined by a haze layer. The same scenario is valid for decreasing the temperature or abundance where the absorption is shifted to lower altitudes. Thus, increasing the temperature, synthetic spectra with lower abundances match the observations and show a lower reduced χ^2 value (and vice versa). Note that this effect is completely degenerate with the location of the haze layer and reference pressure level. Thus, the characteristic shape will shift linearly changing these parameters, denying the determination of the 'real' absolute abundance – temperature values.

However, from this grid of different temperature-abundance spectra, we are able to derive the mean synthetic K I line profile. For this, we determine the best matching line profile at each temperature grid on the characteristic shape (i.e. the red stripe) and calculate the mean line profile by averaging those. The mean synthetic line profile is shown in Fig. 3 with a green dashed line, while the mean synthetic K I line profile prior to the broadening process is presented in a red dashed line. A rotational broadening of ∼3.8 km/s is needed further to the accounted line-broadening mechanisms such as instrumental resolution and atmospheric properties (for instance, temperature and pressure broadening) to match the observational line profile (excluding the planetary rotation).

4.3 Comparison of the synthetic and observational Na I-D lines

We want to compare the resolved Na I-D lines in CSB17 (see Section 2.2) with the Na I-D-absorption lines produced from the synthetic transmission spectra (in the same way as done in Section 4.2 for the K I line). We compare the synthetic and observed absorption lines ±0.62 Å around the Na I-D-line cores corresponding to ∼2× the FWHM (in total 124 spectrally resolved data points for each Na I-D line).

Fig. 5 shows the resulting comparison map for the Na I-D lines (top). Similar to the K I investigation, one can see the degeneracy for the different temperature-abundance combinations due to the haze layer. The middle panel of Fig. 5 shows the corresponding velocity broadening map, where the colour bar indicates the introduced rotational broadening in km/s (the scales are adapted for best visibility). The maps show that the synthetic lines of interest need to be broadened around ∼8–12 km/s to match the observation for both Na I-D lines. We derive the mean synthetic Na I-D-line profiles in the same way as done for the mean synthetic K I line profile. The bottom panel of Fig. 5 shows the resolved line profiles from CSB17 (unbinned = grey solid; binned by 10 pixels for clarity = red dots) and the derived mean synthetic Na I-D-line profiles (dashed black line). The emission peak in the line centre arises due to the fact that only broadened lines from the atmospheric ring are contributing to the final line profile, neglecting the blocked velocity-shifted absorption profiles from the planetary body. For small velocities, this peak vanishes but becomes significant for larger ones. The mean synthetic broadened line profiles match well with the observations. We also show the mean synthetic line profiles before broadening (dashed blue).

5 DISCUSSION

We discuss the different possibilities, which could be the reason for the large difference in the line widths (around a factor of 2)

Downloaded from https://academic.oup.com/mnras/article/498/1/1023/5892592 by Universiteit van Amsterdam user on 15 March 2022

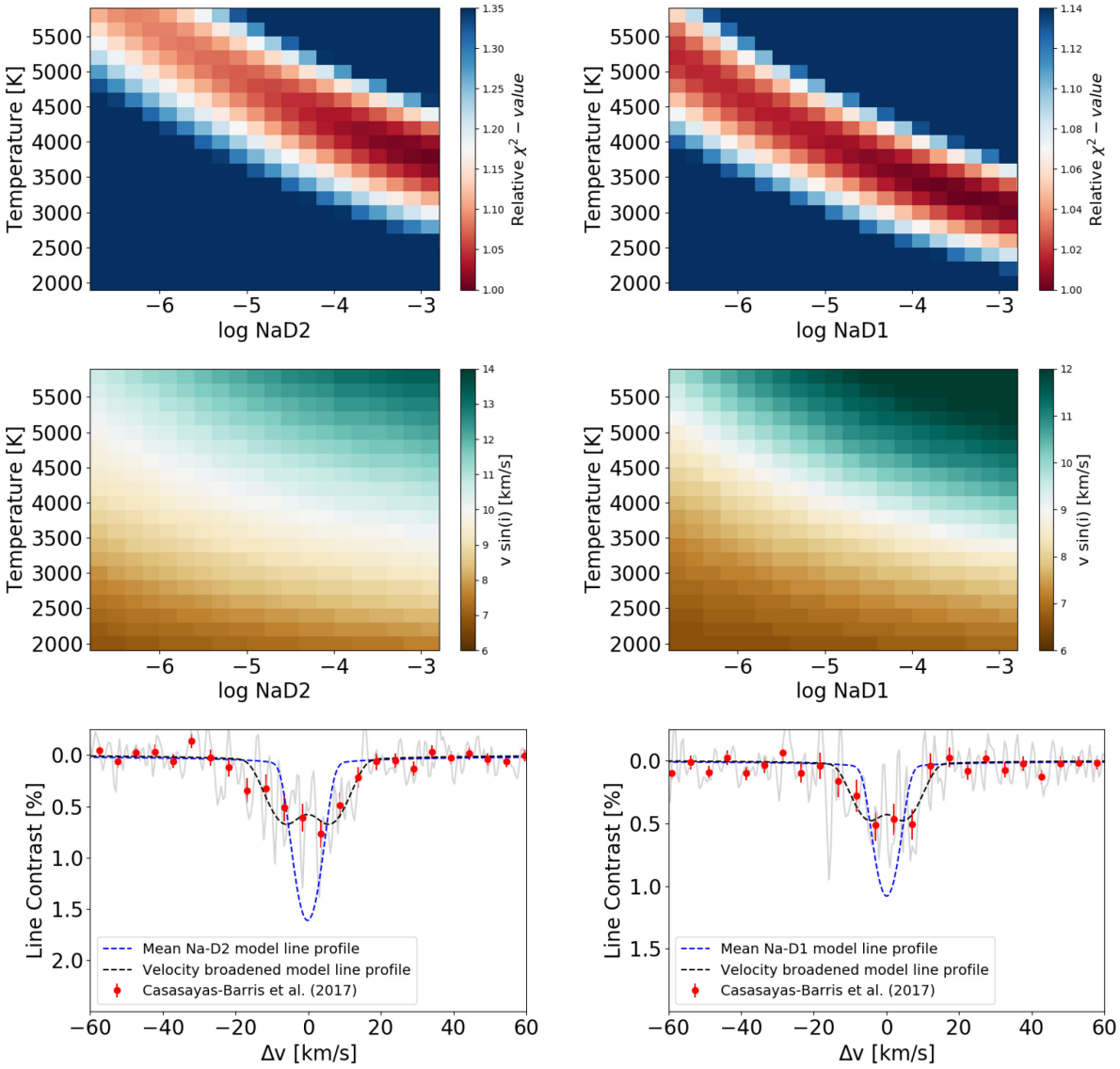

Figure 5. Top panel: Abundance-temperature degeneracy for Na I-D lines, where log NaD2 and log NaD1 are the logarithmic volume mixing ratios. Reduced χ^2 values relative to the best value (colour marked) compare the observational Na I-D profiles with various synthetic spectra, whereby each pixel corresponds to one spectrum comparison. Middle panel: The introduced broadening to the synthetic spectra is shown. The colour bar indicates the broadening value in km/s. Bottom panel: The line contrast over line centre distance in units of velocity is shown for theNa I-D2 line (left) and Na I-D1 line (right). The synthetic mean line profile with (dashed black) and without (dashed blue) introduced broadening. Red dots show the resolved planetary Na I-D lines from Casasayas-Barris et al. (2017) (binned by 10 pixels) and grey show their unbinned data.

for both alkali lines shown in the top panel of Fig. 6, where we show the derived mean synthetic line profiles from this work. The comparison of the resolved Na I-D-line profiles from CSB17 with the synthetically derived ones suggests that the Na I-D lines need to be broadened by velocities in the order of ∼10 km/s, regardless of the atmospheric temperature for the best matching synthetic line profiles, as shown in the middle panel of Fig. 5. Applying a Gaussian fit, the line profiles show an FWHM of ∼22.9 km/s for the Na I-D2 line and ∼18.8 km/s for the Na I-D1 line. Comparing the resolved K I line profile (which has an FWHM of ∼9.4 km/s) with the synthetically derived mean line profile, only a broadening of around 3.8 km/s is needed, which is 2–3 times less compared to that we see for the Na I-D lines. The resolved Na I and K I lines were obtained with different spectrographs (HARPS and PEPSI). Both instruments are high-resolution fibre-fed spectrographs, which are pressure and temperature controlled and observed the alkali lines at similar resolution. The difference in line widths seems to be too large to be explained by potential systematic effects arising from the usage of different instruments. In both cases, one would expect a line broadening of around 2.7 km/s due to the planetary rotation (further to the temperature and pressure broadening introduced into the synthetic line profiles). Taking into account that the alkali lines absorb at higher altitudes around 1–1.3 R_p, this would increase the broadening around a few hundred m/s only. Furthermore, as the planet moves during the transit, the planetary absorption arises at different wavelength positions due to the Doppler shift. At large exposure times, this also introduces a broadening to the observed line profiles regarding the orbital phase. For a 10-min exposure time, this is on the order of a few km/s (at the ingress and egress phases) and decreases down to a few hundred m/s at the

Downloaded from https://academic.oup.com/mnras/article/498/1/1023/5892592 by Universiteit van Amsterdam user on 15 March 2022

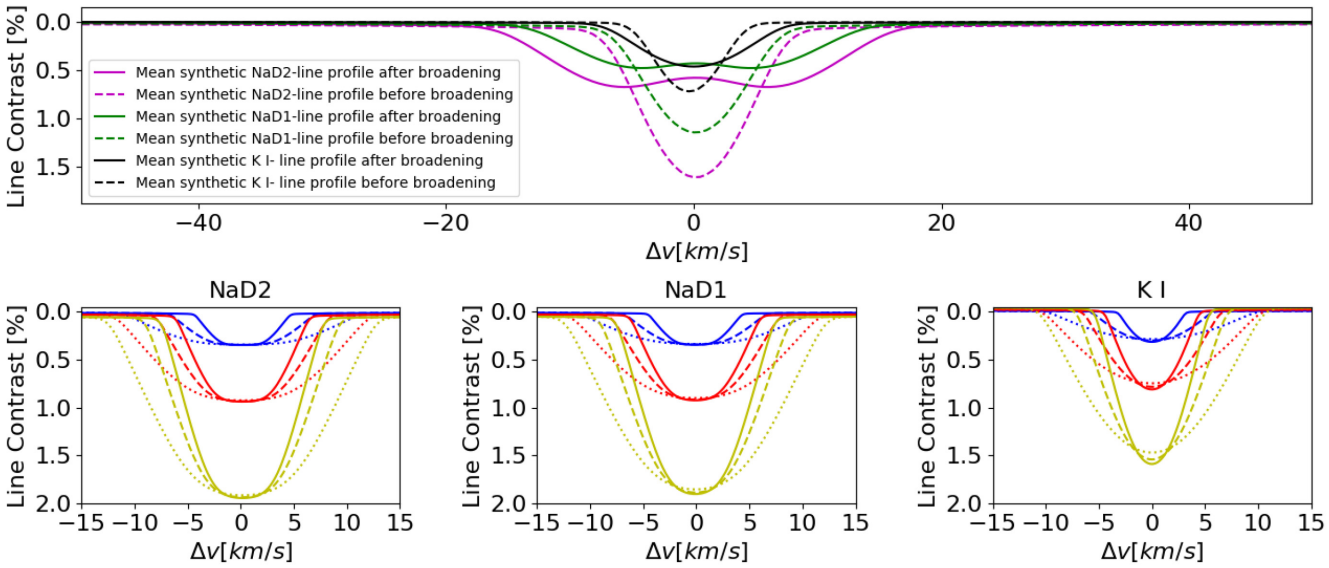

Figure 6. Top panel: Comparison of the mean synthetic Na I-D lines and the K I line from this work. Dashed lines show line profiles before and solid lines after introduced rotational broadening. Bottom panel: Na I-D lines and K I line modelled for isothermal temperature and solar abundance value at 2000 K (blue), 4000 K (red), and 6000 K (yellow) for turbulence velocities of vt of 1 km/s (solid), 10 km/s (dashed), and 20 km/s (dotted). The *x*-axis shows the distance to the line centre in km/s.

mid-transit phase. The line broadening of the resolved K I line can be explained by the orbital motion and the fixed exposure time.

Different atomic lines are found and resolved in other hot- and ultra-hot Jupiter-type planets showing different line widths, e.g. on WASP-49 (Wyttenbach et al. 2017), on Wasp-76 (Seidel et al. 2019), on Wasp-33b (Yan et al. 2019), and on KELT-9b (Yan & Henning 2018; Cauley et al. 2019; Hoeijmakers et al. 2019; Yan et al. 2019; Turner et al. 2020). To the best of our knowledge, so far only Chen et al. (2020) detected another resolved K I line for the exoplanet WASP-52b observed with the high resolution spectrograph ESPRESSO (Echelle SPectrograph for Rocky Exoplanets and Stable Spectroscopic Observations) at the VLT. The authors show the detection of the Na I-D lines with an FWHM (Na I-D2) = 21.6 ± 1.8 km/s and FWHM (Na I-D1) = 11.5 ± 1.6 km/s and the K I-D1 line with an FWHM (K I-D1) = 13.7 ± 3.3 km/s. Even if the FWHM of the Na I-D lines show a strong deviation to each other, their mean FWHM is comparable with the FWHM of the K I-D1 line, opposite to that we see comparing the K I line with the much broader Na I lines in our investigation. Large line widths do not have to be necessarily attributed to being broadened by, e.g. winds, as also other factors determine the line broadening such as pressure- and temperature-broadening or the cross-section of the absorbing species. However, if the observed line broadening cannot be explained by accounting only for these mechanisms, broadening by planetary winds can be considered as the trigger for the enhanced broadening.

An explanation for the strong broadening of the Na I-D lines is shown by Seidel et al. (2020). The authors show that superrotational winds, day- to nightside winds, or vertical wind patterns can introduce strong broadening to the Na I-D lines in the upper atmosphere of HD189733b. The authors propose a possible scenario, where a planetary magnetic field in the order of 50 G propels Na^+-ions via the Lorenz force from a superrotational jet in the lower atmosphere up to the upper atmosphere, which recombines there to neutral Na at the same speed.

Another explanation for the large broadening may be turbulences in the planetary atmosphere. In contrast to the introduced rotational broadening, turbulences would lead to a line broadening by an intrinsic change of the Doppler width, which can be described by:

$$\sigma_{\mathrm{D}} = \frac{\nu_0}{c}\sqrt{\frac{k_{\mathrm{B}}T}{m} + v_{\mathrm{t}}^2}\,. \tag{1}$$

The bottom panel in Fig. 6 shows the effect of turbulent velocities v_{t} on the Na I-D lines and the K I line modelled for solar Na and K abundance value (at an isothermal temperature of 2000 K, 4000 K, and 6000 K for v_{t} of 1 km/s, 10 km/s, and 20 km/s). Introducing rotational broadening, the corresponding equivalent width of the absorption lines remains conserved; thus, deeper lines become broader but shallower. On the other hand, regarding turbulences, this is not the case and the equivalent widths are not conserved. High turbulent velocities flatten the line profiles in the line core region and introduce a characteristic shape, especially at lower temperatures. But also in the case of turbulences, one would expect similar broadening effects for both alkali lines if the turbulences are not variable. Note that a mix of rotational broadening and turbulences may be possible. In this case, the observed line widths would be affected by the degeneracy between rotational broadening, temperature, and turbulences, making the investigation even more complex.

In two recent works, Seidel et al. (2020) and Gebek & Oza (2020) also investigate the broadened Na I-D lines on HD189733b increasing the Doppler width of the lines. Both authors derive velocities even larger than presented in this study for the Na I-D lines. However, a direct comparison of the wind velocities is not possible as the winds are introduced in a different way (Doppler width broadening versus rotational broadening). Changing the Doppler width (i.e. using equation 1), the absorption profile changes as a result of the different velocity distribution of the absorbing Na- atoms, where v_{t} can be also denoted as the microturbulence. On the other way, in case of rotational broadening, the Na atoms in each atmospheric column (in the line of sight) move as a unit and produce an absorption profile, which is velocity shifted with respect to the distance to the rotational

Downloaded from https://academic.oup.com/mnras/article/498/1/1023/5892592 by Universiteit van Amsterdam user on 15 March 2022

axis. The final absorption profile is then the sum of all velocity-shifted line profiles on the atmospheric ring. However, the results are similar in a qualitative way, stating that the Na I-D lines may experience strong broadening on HD189733b.

However, we emphasize that if the broadening of the lines arises from winds or turbulences in the order ∼10 km/s and higher, this would hint on wind velocities larger than the sound speed. But as the atmospheric region where the Na I and K I lines form is below the exobase and thus collisionally dominated, supersonic winds are not possible. Therefore, the inferred velocities should be considered cautiously and rather qualitatively hinting on some broadening mechanisms in the upper atmosphere than quantitatively.

In general, both alkali features were expected to show very similar mixing ratio profiles and to probe similar pressure levels (see figs 7 and 12 in Lavvas & Koskinen 2017) for HD189733b; thus, one could expect similar line broadening. But comparing the absorption level (at similar bandwidths) for Na I shown by Wyttenbach et al. (2015) and K I shown by KEL19, Na I probes ∼27 scale heights and so much higher altitudes compared to K I, which probes ∼13 scale heights, deviating a factor of ∼2 (assuming that the same temperature region is probed). A roughly similar result is inferred comparing the LC of the non-broadened alkali line profiles shown in the top panel of Fig. 6. Hence, Na seems to probe higher altitudes compared to K. However, if Na probes higher temperature around $T_{Na} \sim 2 \times T_K$ (and therefore higher altitude level), the noted difference in scale heights would be in agreement with the expectations. As the atomic mass of K is ∼1.7 times larger than the atomic mass of Na, the Na atoms may be lifted into the upper atmosphere by hydrodynamic motion more easily than K atoms, explaining the difference in altitude. However, advanced modelling effort would be needed to prove this, which is out of the scope of this work.

If the Na I absorption probes much higher altitudes compared to the K I absorption, this could indicate that some mechanism is leading to a broadening to the absorption lines with decreasing pressure level on HD189733b. This is also suggested comparing the K I absorption to other high-resolution investigations regarding wind properties. In case of day- to nightside winds, the largest blueshifts are found for the lightest elements, which probe the lowest pressure regimes such as He-I (Salz et al. 2018) (-3.5 ± 0.4 km/s at the mid-transit) up to the evaporating regime probed by the Ly-α line (Lecavelier des Etangs et al. 2012), where probably evaporation also plays a significant role on such a shift. We find no significant blueshift of the resolved K I line, where we deduce a shift of 0.001 ± 0.01 Å ($\sim 0.04 \pm 0.4$ km/s). However, this cannot exclude the presence of a day- to nightside wind on HD189733b. This value is similar within 2σ to the findings by Louden & Wheatley (2015), who found a velocity shift of $-1.9^{+0.7}_{-0.6}$ km/s investigating the Na I-D lines. Brogi et al. (2016) used the CRIRES (CRyogenic high-resolution InfraRed Echelle Spectrograph) instrument at the VLT to investigate the different molecular absorption features around 2.3 μm during the transit of HD189733b. The authors also probe a lower day- to nightside wind of $-1.7^{+1.1}_{-1.2}$ km/s, which is also consistent within 2σ with our finding. In case of rotational broadening, Brogi et al. (2016) state a rotational velocity of $v_{rot} = 3.4^{+1.3}_{-2.1}$ km/s, which would be in agreement within 1σ with the broadening value needed for the K I line of ∼3.8 km/s. The results of Brogi et al. (2016) have been confirmed by Flowers et al. (2019) analysing the same data set applying 3D GCM (general circulation model) simulations, also being in agreement with our broadening values in sense of wind speed (see their table 1) and blueshift values. As the molecular lines originate at lower altitudes compared to the alkali lines, this appears to be consistent with the fact that some mechanism is producing significant line broadening at low-pressure levels. Comparing the widths of the Na I-D lines with the Hα line (Cauley et al. 2016), both features probe similar altitudes and show similar large widths (Huang et al. 2017), strengthening this picture.

Recently, Gebek & Oza (2020) compared the observational Na I-D lines shown by Wyttenbach et al. (2015) for HD189733b with synthetic transmission spectra computed for different scenarios such as a hydrostatic atmosphere and three evaporative scenarios being an escaping atmosphere, an outgassed cloud sourced by an exomoon and a torus representing circumplanetary material, showing a strong evidence that these lines probe optically thin regions in the atmosphere. Comparing the K absorption by Keles et al. (2019) with their scenarios, the best match is given by a hydrostatic scenario probing an optically thick region. The authors note that their optically thin scenarios are very sensitive to the planetary Na/K ratio, which can vary if this differs from the stellar one. We aim to probe the planetary Na/K ratio and compare this to the stellar Na/K abundance ratio, which we derive in Appendix C. The inferred stellar Na/K abundance ratio is $\log(\mathrm{Na/K}) = \sim 1.2$ similar to the solar value (Asplund et al. 2009). Although the exoplanet could have undergone evolutionary processes changing its Na/K ratio, we expect a similar Na/K ratio for HD189733b, which seems to be an appropriate assumption in the first order (Lavvas et al. 2014). Note that due to the extinction by Earth's atmosphere, high-resolution transit observations are typically not suitable to determine absolute abundances of atmospheric constituents. The continuum information usually gets lost due to re-normalization of the spectra and becomes degenerate with the reference pressure level and transit radius (Benneke & Seager 2012; Heng & Kitzmann 2017; Welbanks & Madhusudhan 2019), whereby under certain circumstances, the degeneracies can be broken (see e.g. Benneke & Seager 2012; Fisher & Heng 2018; Brogi & Line 2019; or Welbanks & Madhusudhan 2019). However, the degeneracies cancel out (for the model assumptions used in this work) deriving the ratio of the abundances, such as the Na/K ratio, unless the temperature at which the lines form is different. We roughly estimate the Na/K ratio by comparing the upper panel of Figs 4 and 5 assuming that both features arise at the same atmospheric temperature and use the abundance value for the best matching model (i.e. the model with the lowest reduced χ^2 value). For the temperature range of 3400–5000 K, we infer a planetary $\overline{Na\,i}/K\,i$ ratio, which is ∼20–400 times higher than the stellar Na/K abundance ratio. Note, that if Na originates at higher temperature than K, the planetary Na/K abundance ratio will decrease to a lower level, down to the solar Na/K abundance value. We emphasize here that the roughly estimated Na/K values should be considered only as a hint that the alkali lines may probe different atmospheric temperature regions, as the inferred Na/K ratio has large uncertainties and relies on different assumptions (which we present in Appendix B). Furthermore, such an increased abundance ratio seems to be unlikely to be present either in the protoplanetary disc or the atmosphere of the planet taking into account primordial elemental abundances and alkali chemistry as discussed for the hot Jupiter HD209458b in Lavvas et al. (2014), which also orbits a solar metallicity star. Furthermore, a strong variation in the alkali abundances due to depletion, e.g. by ionization processes as well as condensation processes seems to be unreasonable. Condensation for K and Na would be expected below an atmospheric temperature of 1000 K for both species in a very similar way (Lavvas & Koskinen 2017), where both alkalis can condense into various different solids and liquids. Likely candidates (see e.g. Marley et al. 2013) are sodium sulfide (Na2S) and potassium chloride (KCl). The former condenses around 900 K in a solar metallicity atmosphere at 0.1 bar, while the latter requires slightly lower temperatures (about 720 K). For an

Downloaded from https://academic.oup.com/mnras/article/498/1/1023/5892592 by Universiteit van Amsterdam user on 15 March 2022

extended presentation of alkali chemistry, we refer here to Lavvas et al. (2014). In the case of photoionization, K (∼4.34 eV) has only slightly lower ionization potential than Na (∼5.14 eV) (Fortney et al. 2003; Barman 2007), making also this process unlikely to be the reason for such a difference.

6 SUMMARY & CONCLUSION

We compared previously observed high-resolution Na I (Casasayas-Barris et al. 2017) and K I (Keles et al. 2019) absorption in the atmosphere of HD189733b with synthetic transmission spectra modelled for a variety of temperature and abundance values. The comparison of the Na I-D lines shows that the observed Na I-D-line widths are much larger than the modelled ones. The Na I-D lines have to be broadened by velocities in the order of ∼10 km/s to match the observations if only rotational broadening is taken into account. To compare the K I line with the synthetic transmission spectra, we used the previous high-resolution observation by KEL19 and resolved the K I absorption from the data. The K I line profile shows a broadening comparable with the modelled synthetic line profiles, which is significantly less in comparison to the Na I-D lines. Comparing to different investigations, there is a hint that the line widths show stronger broadening with increasing altitude: starting from molecular absorption signature from the lower atmosphere showing weak or even no significant broadening effects (Brogi et al. 2016) up to the slightly larger broadened K I line (this work) and even to higher altitudes where the Na I-D lines (Wyttenbach et al. 2015; Louden & Wheatley 2015; Barnes et al. 2016; Casasayas-Barris et al. 2017; Borsa & Zannoni 2018; Seidel et al. 2020) and the Hα line (Cauley et al. 2016) show very large broadening. The same picture is drawn comparing the wavelength shifts introduced by a probably day- to nightside wind, which shows stronger blueshifts for the lines emerging at lower pressure levels. This hints that the main K I absorption may arise from lower altitudes than the Na I absorption. Estimating the planetary Na/K ratio and comparing this to the derived stellar Na/K ratio, HD189733b would possess a very high supersolar atmospheric Na/K ratio if Na and K trace the same atmospheric temperature for the model assumptions used in this work. However, the derived Na/K ratio depends on several assumptions and is such enhanced that this scenario seems to be very unlikely. In case that K traces lower altitudes at a cooler temperature compared to Na, the planetary Na/K ratio can coincide with the stellar Na/K ratio being in agreement with other studies such as Welbanks et al. (2019), which seems to be a more likely scenario.

Another high-resolution and high-S/N transit observation, which covers the wavelength range of different atomic and molecular species, would be needed to compare the broadening mechanisms to avoid artefacts attributed to the stellar activity, different instrumentation, or even variable weather conditions on the exoplanet.

ACKNOWLEDGEMENTS

We sincerely thank N. Casasayas Barris for sharing the high-resolution data including the resolved Na I-D lines.

KGS thanks the German Federal Ministry (BMBF) for the year-long support for the construction of PEPSI through their Verbundforschung grants 05AL2BA1/3 and 05A08BAC as well as the State of Brandenburg for the continuing support of LBT and PEPSI (see https://pepsi.aip.de/). LBT Corporation partners are the University of Arizona on behalf of the Arizona university system; Istituto Nazionale di Astrofisica, Italy; LBT Beteiligungsgesellschaft, Germany, representing the Max-Planck Society, the Leibniz-Institute for Astrophysics Potsdam (AIP), and Heidelberg University; the Ohio State University; and the University of Notre Dame, University of Minnesota, and University of Virginia.

LP is supported by funding from the European Research Council (ERC) under the European Union's Horizon 2020 research and innovation programme (grant agreement no. 679633; Exo- Atmos).

XA is grateful for the financial support from the Potsdam Graduate School (PoGS) in form of a doctoral scholarship.

JVS is supported by funding from the European Research Council (ERC) under the European Union's Horizon 2020 research and innovation program (project FOUR ACES; grant agreement no. 724427).

DATA AVAILABILITY

The data underlying this article will be shared on reasonable request to the corresponding author.

REFERENCES

Allard N. F., Spiegelman F., Kielkopf J. F., 2016, A&A, 589, A21
Allart R., Lovis C., Pino L., Wyttenbach A., Ehrenreich D., Pepe F., 2017, A&A, 606, A144
Asplund M., Grevesse N., Sauval A. J., Scott P., 2009, ARA&A, 47, 481
Barman T., 2007, ApJ, 661, L191
Barnes J. R., Haswell C. A., Staab D., Anglada-Escudé G., 2016, MNRAS, 462, 1012
Baudino J.-L., Bézard B., Boccaletti A., Bonnefoy M., Lagrange A.-M., Galicher R., 2015, A&A, 582, A83
Benneke B., Seager S., 2012, ApJ, 753, 100
Borsa F., Zannoni A., 2018, A&A, 617, A134
Bourrier V. et al., 2018, Nature, 553, 477
Bower D. J., Kitzmann D., Wolf A. S., Sanan P., Dorn C., Oza A. V., 2019, A&A, 631, A103
Brogi M., Line M. R., 2019, AJ, 157, 114
Brogi M., Kok R. J. d., Albrecht S., Snellen I. A. G., Birkby J. L., Schwarz H., 2016, ApJ, 817, 106
Burrows A., Volobuyev M., 2003, ApJ, 583, 985
Cameron A. C., Bruce V. A., Miller G. R. M., Triaud A. H. M. J., Queloz D., 2010, MNRAS, 403, 151
Casasayas-Barris N. et al., 2020, A&A, 635, A206
Casasayas-Barris N., Palle E., Nowak G., Yan F., Nortmann L., Murgas F., 2017, A&A, 608, A135
Cauley P. W., Redfield S., Jensen A. G., Barman T., 2016, AJ, 152, 20
Cauley P. W., Kuckein C., Redfield S., Shkolnik E. L., Denker C., Llama J., Verma M., 2018, AJ, 156, 189
Cauley P. W., Shkolnik E. L., Ilyin I., Strassmeier K. G., Redfield S., Jensen A., 2019, AJ, 157, 69
Cegla H. M., Lovis C., Bourrier V., Beeck B., Watson C. A., Pepe F., 2016, A&A, 588, A127
Charbonneau D., Brown T. M., Noyes R. W., Gilliland R. L., 2002, ApJ, 568, 377
Chen G., Casasayas-Barris N., Pallé E., Yan F., Stangret M., Cegla H. M., Allart R., Lovis C., 2020, A&A, 635, A171
Czesla S., Klocová T., Khalafinejad S., Wolter U., Schmitt J. H. M. M., 2015, A&A, 582, A51
Draine B. T., 2011, Physics of the Interstellar and Intergalactic Medium, Princeton University Press, Princeton, New Jersey
Dravins D., Gustavsson M., Ludwig H.-G., 2018, A&A, 616, A144
Fisher C., Heng K., 2018, MNRAS, 481, 4698
Flowers E., Brogi M., Rauscher E., Kempton E. M.-R., Chiavassa A., 2019, AJ, 157, 209
Fortney J. J., Sudarsky D., Hubeny I., Cooper C. S., Hubbard W. B., Burrows A., Lunine J. I., 2003, ApJ, 589, 615
Fossati L., Koskinen T., Lothringer J. D., France K., Young M. E., Sreejith A. G., 2018, ApJ, 868, L30
Gaidos E., Kitzmann D., Heng K., 2017, MNRAS, 468, 3418

Downloaded from https://academic.oup.com/mnras/article/498/1/1023/5892592 by Universiteit van Amsterdam user on 15 March 2022

Gebek A., Oza A. V., 2020, MNRAS, preprint (arXiv:2005.02536)
Gibson N. P. et al., 2020, MNRAS, 493, 2215
Gray R. O., Corbally C. J., 1994, AJ, 107, 742
Gustafsson B., Edvardsson B., Eriksson K., Jørgensen U. G., Nordlund, Å., Plez B., 2008, A&A, 486, 951
Heng K., Kitzmann D., 2017, MNRAS, 470, 2972
Hoeijmakers H. J. et al., 2018, Nature, 560, 453
Hoeijmakers H. J. et al., 2019, A&A, 627, A165
Huang C., Arras P., Christie D., Li Z.-Y., 2017, ApJ, 851, 150
Jensen A. G., Redfield S., Endl M., Cochran W. D., Koesterke L., Barman T. S., 2011, ApJ, 743, 203
Keles E. et al., 2019, MNRAS Lett., 489, L37
Khalafinejad S. et al., 2017, A&A, 598, A131
Klocová T., Czesla S., Khalafinejad S., Wolter U., Schmitt J. H. M. M., 2017, A&A, 607, A66
Lavvas P., Koskinen T., 2017, ApJ, 847, 32
Lavvas P., Koskinen T., Yelle R. V., 2014, ApJ, 796, 15
Lecavelier des Etangs A. et al., 2012, A&A, 543, L4
Louden T., Wheatley P. J., 2015, ApJ, 814, L24
Marley M. S., Ackerman A. S., Cuzzi J. N., Kitzmann D., 2013, Comparative Climatology of Terrestrial Planets, Clouds and Hazes in Exoplanet Atmospheres, University of Arizona Press, Tucson, Arizona
Mayor M. et al., 2003, Messenger, 114, 20
McLaughlin D. B., 1924, ApJ, 60, 22
Montes D. et al., 2018, MNRAS, 479, 1332
Pino L. et al., 2018a, A&A, 612, A53
Pino L. et al., 2018b, A&A, 619, A3
Plez B., 2012, Astrophysics Source Code Library, record ascl:1205.004.
Pont F., Sing D. K., Gibson N. P., Aigrain S., Henry G., Husnoo N., 2013, MNRAS, 432, 2917
Redfield S., Endl M., Cochran W. D., Koesterke L., 2008, ApJ, 673, L87
Rossiter R. A., 1924, ApJ, 60, 15
Ryabchikova T., Piskunov N., Kurucz R. L., Stempels H. C., Heiter U., Pakhomov Y., Barklem P. S., 2015, Phys. Scr, 90, 054005
Salz M. et al., 2018, A&A, 620, A97
Seager S., Sasselov D. D., 2000, ApJ, 537, 916
Seidel J. V. et al., 2019, A&A, 623, A166
Seidel J. V., Ehrenreich D., Pino L., Bourrier V., Lavie B., Allart R., Wyttenbach A., Lovis C., 2020, A&A, 633, A86
Showman A. P., Fortney J. J., Lewis N. K., Shabram M., 2013, ApJ, 762, 24ferent assumptions, which will be
Sing D. K. et al., 2016, Nature, 529, 59
Snellen I. A. G., de Kok R. J., de Mooij E. J. W., Albrecht S., 2010, Nature, 465, 1049
Southworth J., 2010, MNRAS, 408, 1689
Strassmeier K. G. et al., 2015, Astron. Nachr., 336, 324
Strassmeier K. G., Ilyin I., Steffen M., 2018a, A&A, 612, A44
Strassmeier K. G., Ilyin I., Weber M., 2018b, A&A, 612, A45
Turner J. D. et al., 2020, ApJ, 888, L13
Welbanks L., Madhusudhan N., 2019, AJ, 157, 206
Welbanks L., Madhusudhan N., Allard N. F., Hubeny I., Spiegelman F., Leininger T., 2019, ApJ, 887, L20
Wyttenbach A. et al., 2017, A&A, 602, A36
Wyttenbach A., Ehrenreich D., Lovis C., Udry S., Pepe F., 2015, A&A, 577, A62
Yan F. et al., 2019, A&A, 632, A69
Yan F., Henning T., 2018, Nature Astron., 2, 714
Yan F., Pallé E., Fosbury R. A. E., Petr-Gotzens M. G., Henning T., 2017, A&A, 603, A73

APPENDIX A: SYNTHETIC TRANSMISSION SPECTRA

We compute theoretical transmission spectra by calculating the effective tangent height and the wavelength-dependent, apparent planetary radius with the `Helios-o` model as described in Bower et al. (2019) or Gaidos, Kitzmann & Heng (2017). The isothermal atmosphere is divided equidistantly in log(P) into 200 layers from 10 bar to 10^{-10} bar. The spectra are computed at a constant resolution of 0.01 cm^{-1} in the wavenumber range between 10 000 cm^{-1} and 20 000 cm^{-1}.

The opacity sources that are included in the calculations are the collision-induced absorption of H_2–H_2 and H_2–He pairs, the D_1 and D_2 resonance lines of K I and Na I, and molecular Rayleigh scattering of H_2 and He. The line strengths S for the Na I and K I resonance lines are obtained via

$$S = \frac{g_2 A_{21}}{8\pi \nu_0^2 Q} \exp\left(-\frac{E_1}{k_B T}\right)\left[1 - \exp\left(-\frac{hc\nu_0}{k_B T}\right)\right], \quad \text{(A1)}$$

where g_2 is the statistical weight of the upper level, A_{21} the Einstein A-coefficient, ν_0 the wavenumber of the transition, E_1 the energy of the lower level, Q the partition function, and T the temperature. The values for g_2 and A_{21} are taken from Draine (2011), while E_1 is zero because the resonance lines are ground-level transitions. The line profile is modelled by a Voigt profile, consisting of a Doppler core and Lorentzian line wings, where the standard deviation of the Doppler profile σ_D is given by

$$\sigma_D = \frac{\nu_0}{c}\sqrt{\frac{k_B T}{m}}, \quad \text{(A2)}$$

with the molecular mass of the species m. The Na I and K I resonance lines are well known for possessing a far-wing line profile that is non-Lorentzian (e.g. Burrows & Volobuyev 2003; Allard, Spiegelman & Kielkopf 2016). We approximate this behaviour by using the analytic fits to the Burrows & Volobuyev (2003) line profiles according to Baudino et al. (2015). We note, however, that because of the strong aerosol scattering slope, the far wings of these lines are practically invisible and only the thermally broadened Doppler cores are located above the spectrum's continuum level.

APPENDIX B: CAUTIONS ON THE ESTIMATED PLANETARY NA/K ABUNDANCE RATIO

The estimated planetary Na/K abundance ratio in this work is based on different assumptions, which will be discussed here. The temperature distribution at the terminator may not be constant as expected from the isothermal profiles; thus, it can affect the abundance ratio, as the line cores form at a much higher temperature than the line wings (Huang et al. 2017). We estimate the Na/K ratio from Figs 4 and 5, where we introduced rotational broadening. If the line broadening is a result of turbulences, the equivalent width of the absorption lines is not conserved; thus, the line widths will be larger without an increase in line depth, which will lead to overestimation of the Na/K abundance ratio. Furthermore, the synthetic line profiles depend on the functional form of the continuum, which is determined by the aerosol layer. Changing the functional form of the continuum will also affect the results presented here. For instance, Welbanks et al. (2019) derived the atmospheric abundances of Na and K for several planets and compared them to those of their host stars. In this study, the authors also investigated the planet HD189733b using *HST* data acquired with the STIS instrument as presented by Sing et al. (2016). The authors infer similar stellar and planetary Na and K abundances based on their retrieval analysis of these data. However, inspecting panel 15 on their fig. 2, the retrieval results are based only on 2 data points around the K I line, resulting probably in a debatable conclusion. However, as the derived planetary Na/K abundance ratio is much larger than what would be expected, we only state the estimated supersolar Na/K ratio on HD189733b as a hint that Na and K may originate at different atmospheric

Downloaded from https://academic.oup.com/mnras/article/498/1/1023/5892592 by Universiteit van Amsterdam user on 15 March 2022

regimes, as the aforementioned effects have a strong impact on the result, similar to non-LTE effects, which could also play a role. Note that high-resolution observations are not always described well by simple theoretical models (such as the one employed here) and mismatches between observational and modelled line profiles can be found, e.g. in Hoeijmakers et al. (2018) and Hoeijmakers et al. (2019). While in those studies the Fe lines match extremely well with the theoretical predictions, the Fe^{+} measurements, on the other hand, deviate by quite a large degree. It is obvious that the theoretical models lack some of the physics to describe the spectral lines or the chemical abundances in the very high atmosphere properly.

APPENDIX C: THE STELLAR NA AND K ABUNDANCE RATIO

The metallicity of HD 189733 is known to be roughly solar, according to previously published investigations, and so is its Na abundance, e.g. [Na/H] $= -0.04 \pm 0.06$, [Fe/H] $= -0.10 \pm 0.03$ (Montes et al. 2018). However, even if the Na/K abundance ratio of HD189733 is expected to be solar (Welbanks & Madhusudhan 2019), we could not find similar abundance information about K. We decided therefore to derive an estimate of the stellar K abundance based on the available PEPSI spectrum. For this purpose, we selected the clean K I line at 7699 Å and compared its profile with synthetic spectra computed for a set of different K abundances, $A(\mathrm{K})$,[2] between 4.5 and 5.5, centred on the solar abundance of $A(\mathrm{K}) = 5.03 \pm 0.09$ (Asplund et al. 2009). The comparison is shown in the bottom panel of Fig. C1.

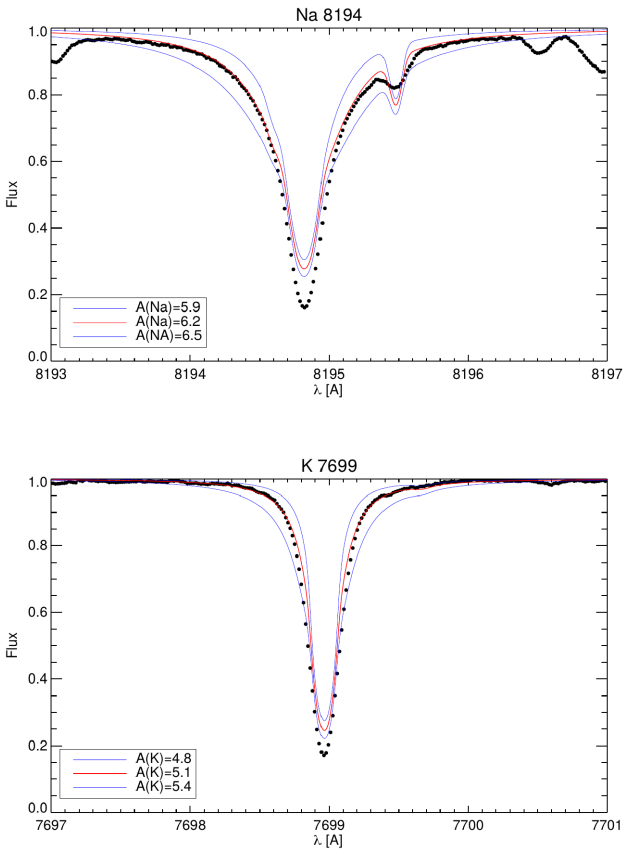

Figure C1. Comparison of Na line at 8195 Å (top) and the 7699 Å K I line (bottom) from PEPSI spectra with the spectrum synthesis model based on a standard 1D model atmosphere. 'A' denotes the logarithmic abundance value.

The spectrum synthesis is based on a standard 1D model atmosphere taken from the MARCS grid (Gustafsson et al. 2008) with parameters $T_{\mathrm{eff}} = 5000$ K, $\log g = 4.5$, [Fe/H] $= 0.0$, and $\xi_{\mathrm{micro}} = 1.0$ km/s, which represents HD 189733 reasonably well (cf. stellar parameters compiled by Southworth 2010). This model atmosphere was then used by the line formation code Turbospectrum[3] (Plez 2012) that generates synthetic line profiles for a given set of atomic parameters characterizing the spectral line in question. The atomic line data were taken from the VALD3 database[4] (Ryabchikova et al. 2015, and updates), including updated pressure-broadening constants.

Comparing observed and synthetic line profiles, we notice that the line cores of the synthetic spectra are too shallow. This presumably indicates that the assumption of LTE (Local Thermodynamic Equilibrium) is not a valid approximation in the core of this rather strong K I line (line depth $d > 0.8$). However, we may assume that the wings of the line, where $d < 0.2$, form in LTE conditions and can be used to estimate the K abundance from a comparison with the synthetic LTE spectra. The best match of the wings is found for $A(\mathrm{K}) = 5.1 \pm 0.1$. This result is fully consistent with the expectation that HD 189733 has a solar K abundance. As a sanity check, we have performed the same exercise with the Na line at 8194 Å. The comparison is shown in the top panel of Fig. C1. Also, in this case, the observed line core is much deeper than the model results for the same reason responsible for the mismatch in the K I line discussed above. Fitting the line wings, we deduce $A(\mathrm{Na}) = 6.2 \pm 0.1$, which is fully consistent with the solar photospheric abundance of $A(\mathrm{Na}) = 6.24 \pm 0.04$ (Asplund et al. 2009). We conclude that the stellar Na/K abundance ratio is indistinguishable from solar, $N(\mathrm{Na})/N(\mathrm{K}) \approx 16$.

[2] $A(\mathrm{X}) = \log(N(\mathrm{X})/N(\mathrm{H})) + 12$
[3] ttps://github.com/bertrandplez/Turbospectrum2019
[4] http://vald.astro.uu.se/

This paper has been typeset from a TEX/LATEX file prepared by the author.

Downloaded from https://academic.oup.com/mnras/article/498/1/1023/5892592 by Universiteit van Amsterdam user on 15 March 2022